Journal of Solid State Chemistry **167,** 386–392 (2002)
doi:10.1006/jssc.2002.9580

Spectroscopic and Crystal Field Investigation of Kramers-Ions: Nd^{3+}:YAB—a Case Study of the Crystal Field Structure of the $^4I_{9/2}$ Ground State[1]

M. H. Bartl,*,[2] E. C. Fuchs,* K. Gatterer,* H. P. Fritzer,* M. Bettinelli,† and A. Speghini†

*Institut für Physikalische und Theoretische Chemie, Graz University of Technology, Austria; and †Dipartimento Scientifico e Tecnologico, Università di Verona, Italy

Received October 18, 2001; in revised form January 11, 2002; accepted March 8, 2002

IN HONOR OF PROFESSOR GALEN STUCKY ON THE OCCASION OF HIS 65TH BIRTHDAY

Single crystals of yttrium aluminium borate, $YAl_3(BO_3)_4$, (referred to as YAB) doped with 20 and 40 mol% of Nd^{3+} were grown using a flux growth method. Inconsistencies in regard to the reported ground state splitting of the doped material are pointed out. A consistent splitting and assignment of the $^4I_{9/2}$ ground state levels of the Kramers-ion Nd^{3+} was obtained by a combination of both, temperature-dependent $^4I_{9/2} \rightarrow {}^2P_{1/2}$ polarized absorption spectroscopy and room temperature $^4F_{3/2} \rightarrow {}^4I_{9/2}$ luminescence spectroscopy. The group theoretical implications of the crystal field analysis are considered and discussed.

Key Words: **yttrium aluminum borate; neodymium; Kramers-ion; polarized electronic spectroscopy; luminescence; crystal field analysis; group theory.**

1. INTRODUCTION

For several reasons the yttrium aluminum borate (YAB) crystal is an interesting and technologically relevant subject of research. On the one hand, the material has excellent chemical and physical properties, e.g., a high hardness compared with the yttrium aluminum garnets, a high UV transparency, a high radiation damage threshold, and it is not prone to develop color centers. These properties have already stimulated the exploration of its potential use as a laser host material in the recent past (1–7). On the other, hand it has been shown that YAB is an ideal self-frequency doubling crystal (4, 5, 8), with a rather high non-linear optical coefficient and a large stimulated emission cross section at 1062 nm. In combination with the four-level laser ion Nd^{3+} it can therefore be used to convert the NIR laser emission into the green spectral range. However, by looking at the literature of the Nd^{3+}:YAB system it becomes evident that there are inconsistencies concerning both the positions and assignments of crystal field states of Nd^{3+} as reported by different authors. The energies of the five two-fold degenerate crystal field split energy levels of the $^4I_{9/2}$ ground state of Nd^{3+} denoted in this contribution as $^4I_{9/2}$(a), $^4I_{9/2}$(b), $^4I_{9/2}$(c), $^4I_{9/2}$(d), and $^4I_{9/2}$(e), in order of ascending energy, are usually determined by means of luminescence spectroscopy. The transition $^4F_{3/2} \rightarrow {}^4I_{9/2}$ is normally used to work out the ground state Stark splitting (1, 2, 6, 7, 9–13). Some of these reported results for the ground state splitting are collected in Table 1. It is interesting to observe that for most of the excited states the agreement of the experimentally determined energies is much better.

Here, we report on the determination of the $^4I_{9/2}$ ground state crystal field splitting of Nd^{3+} in YAB single crystals using the well-established method of temperature dependent absorption spectroscopy, e.g. (14–16). By comparing the energies of the $^4I_{9/2}$ Stark levels obtained by this technique with that obtained by room-temperature luminescence spectroscopy measurements it is demonstrated that ambiguities resulting from the luminescence data can be solved and an unambiguous assignment of the $^4I_{9/2}$ crystal field states is obtained.

Apart from the possible technological applications of the YAB crystals doped with Nd^{3+} laser material, such a study is also very interesting from a theoretical point of view. The odd number of *f* electrons of this 4*f* - ion leads to half-odd integer values of the total electronic angular momentum quantum numbers *J*. Therefore, this requires the use of the double group $^2D_3$ in order to perform the symmetry analysis properly. In this context, it is worth mentioning that the character tables and direct product tables of $^2D_3$ found in the literature do not always agree with each other, and some of them are obviously wrong. For the benefit of the reader

[1] Dedicated to Professor Galen D. Stucky on the occasion of his 65th birthday.

[2] To whom correspondence should be addressed. Present address: Department of Chemistry and Biochemistry, University of California, Santa Barbara, CA 93106, USA. fax: + 1-805-893-4120. E-mail: bartl@chem.ucsb.edu.

0022-4596/02 $35.00

TABLE 1
$^4I_{9/2}$ Ground State Splitting of Nd_{3+} in Nd:YAB Obtained from $^4F_{3/2} \rightarrow {}^4I_{9/2}$ Luminescence Spectra by Different Authors

$^4I_{9/2}$ ground state splitting (cm^{-1})	Nd^{3+} content (mol%)	Reference
0, 105, 158, 324, 324	4	(9)
0, 52, 134, 218, 285	—	(10)
0,19, 108, 236, 286	100	(11, 12)
0, 48, 109, 165, 289	2	(1)
0, 49, 147, 271, 323	100	(6, 7)
0, 49, 147, 218, 299	20, 40	This work

Note. The relative energies of the five Stark levels $^4I_{9/2}$(a), $^4I_{9/2}$(b), $^4I_{9/2}$(c), $^4I_{9/2}$(d), and $^4I_{9/2}$(e), are listed in cm^{-1}. The Nd^{3+} content, where known, is indicated.

we present the tables relevant for the spectroscopy of our work in this contribution.

2. EXPERIMENTAL

2.1. Crystal Growth

Single crystals of Nd^{3+}:YAB with 20 and 40 mol% Nd^{3+} were grown from a flux consisting of water-free K_2SO_4 (99%) and MoO_3 (99.5%) in the molar ratio of 1:3 (17). Appropriate amounts of Y_2O_3 (99.999%), Al_2O_3 (98%), B_2O_3 (97%), and Nd_2O_3 (99.9%) were weighed and then mixed with the flux in the ratio 40:60 (wt%). The mixture was ground to a fine powder and filled in a 25 ml platinum crucible covered with a tight fitting platinum lid to avoid too fast evaporation of the flux. The crucible was placed in a front loaded electric resistance furnace (Nabertherm; equipped with "Super Kanthal" elements; max. temperature: $\approx 1800°C$) equipped with an electronic controller (Nabertherm: Program Controller C42). Good-quality crystals were obtained when the crucible was put into a support made of firebricks, which ensures that the bottom of the crucible is not in direct contact with the furnace (heat transfer by radiation only). The optimized temperature profile for crystal growth consisted of an increase to 1120°C with a heating rate of 300°C/h. A soak period of 3 h at this temperature was followed by a cooling period down to 850°C with a cooling rate of 1°C/h. At 850°C the furnace was switched off and the platinum crucible cooled down to room temperature. The Nd^{3+}:YAB single crystals were isolated from the remaining flux by boiling 1–2 h in KOH (8 M). A typical Nd^{3+}:YAB crystal obtained in this way is shown in Fig. 1.

The size of the crystals was between 1 and 5 mm in length and up to about 3 mm in diameter. Flux inclusions—which are virtually unavoidable with this preparation technique—were concentrated in the surface layer and could be removed by grinding and polishing the crystals prior to the optical measurements. Grinding and polishing was performed in four steps. First, the crystals were ground on a diamond disk (grain size 20 μm; ∅ 20 cm; Struers) with water as lubricant. In the second step, a slurry of SiC (grit 1000; Buehler) and water on a normal window-glass plate was used. Before polishing the crystals were cleaned in an ultrasound bath. In order to remove fine scratches on the surface created by the grinding process the crystals were polished on polishing cloths (Texmet 1000; Buehler) with an alumina slurry (Al_2O_3; 0.3 μm; Buehler).

2.2. Polarized VIS Absorption Spectroscopy

Optical spectra in the visible range (850–320 nm, corresponding to 11,800–31,250 cm^{-1}) were recorded with a UV-VIS spectrometer (Bruins Instruments, Omega-10). The spectrometer is equipped with a $f = 0.25$ m Czerny–Turner double monochromator and a photomultiplier (R 374). In order to record polarized spectra a polarizer equipped with Glan-Thompson calcite polarizing prisms (Melles Griot) was used. The spectra were recorded in the single-beam mode in order to use the same light path for both the reference and the sample spectra and eliminate possible interference from different optical surfaces in the two beams. Up to 1000 spectra of a crystal were accumulated in each run in order to increase the signal-to-noise ratio substantially. The spectral resolution achieved is about 4 cm^{-1}. For low-temperature measurements (10 K), the same spectrometer was used in combination with a closed-cycle helium cryostat (Leybold-Heraeus; ROK-10).

2.3. Laser-Excited Luminescence Spectroscopy

For the laser-induced luminescence spectroscopy no prior treatment of the crystals was necessary and thus the biggest crystals were used regardless of any flux inclusions. The excitation of the crystals was performed using the 488.0 nm

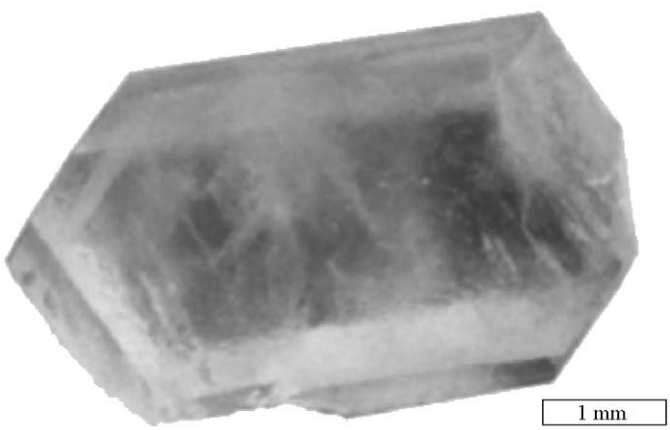

FIG. 1. Enlarged view of an as-grown Nd^{3+}:YAB (20 mol%) single crystal. The length of the white bar is 1 mm.

line of an argon ion laser (Spectra Physics; Stabilite 2017). The emitted radiation was collected with a 90° geometry using a Dilor Superhead coupled to a glass fiber guide. The signal was analyzed by a monochromator (Jobin Yvon HR 460; ISA Division d'Instruments S.A.) and a CCD detector. All the laser-induced measurements were performed at room temperature.

3. RESULTS AND DISCUSSION

3.1. Group Theoretical Implications—the $^2D_3$ Double Group

The structure of Nd^{3+}:YAB is known from X-ray crystal structure investigations (18–20). The material is isostructural with the mineral huntite and belongs to the $R32$ space group. Nd^{3+} ions occupy Y^{3+} sites with D_3 micro-symmetry. Since the ground state electron configuration of Nd^{3+} ([Xe]$4f^3 5s^2 5p^6$) bears an odd number of electrons in the partly filled 4*f*-shell, the total spin quantum number S as well as the total electronic angular momentum quantum number J of all the Nd^{3+} states are half-odd integer. Such ions are called "Kramers-ions" since in the absence of external magnetic fields all the energy levels remain at least two-fold degenerate (this is also called Kramers' degeneracy). For a systematic and consistent symmetry analysis of the Kramers-ion Nd^{3+} one has to use not one of the ordinary points or space groups but the so-called "double groups" denoted ^2G in the notation of (21), i.e., $^2D_3$ is needed in our work. Although these groups were investigated by many authors, in contrast to the ordinary groups unpleasant ambiguities (nomenclature), errors and wrong character tables [see, e.g. (22)] are still common in the literature. Therefore, we worked out the character table of the $^2D_3$ double group as well as the electric dipole transition selection rules derived from the scratch.

The general features of double groups (^2G), which have twice the order of the crystallographic groups G, were outlined as early as 1929 by Bethe (23) and later by Opechowski (24). The double groups ^2G are subgroups of the special unitary group $SU(2)$ and can therefore be regarded as inverse images, f^{-1} say, in $SU(2)$ of either the continuous group $SO(3)$ or one of its subgroups G:

$$^2G = f^{-1}(G). \qquad [1]$$

Following the rules given in (21) and (22), Eq. [1] and the period splitting rules given in (21) the structure of the dihedral double group $^2D_3$ and its character table (Table 2) are derived unambiguously.

By application of the group-theoretical reduction formula onto the character system each of the basis functions $|J, M\rangle$ corresponding to the Russell–Saunders states $^{2S+1}L_J$ with half-odd integer J-values (collected in the last column of Table 2) is reduced into a direct sum of the irreducible representations of $^2D_3$. Here, it should be emphasized that all the basis functions with half-odd integer J-values transform in $^2D_3$ either according to the two one-dimensional complex-conjugate irreducible representations $^2\Gamma_3$ and $^2\Gamma_4$, or the two-dimensional irreducible representation $^2\Gamma_6$. This behavior is closely related to the action of the time-reversal operator on a physical system like the Nd^{3+}:YAB material in addition to the action of the $^2D_3$ spatial operators. In principle we should work in a larger symmetry group than $^2D_3$. Fortunately, Wigner [in (25)] has shown that the effect of time-reversal symmetry on a physical system, which implies the invariance of its Hamilton operator in the absence of external magnetic fields, can be studied in the double group alone. However, this additional symmetry implies in our case some modifications in using the character table. The irreps $^2\Gamma_3$ and $^2\Gamma_4$ in $^2D_3$ are the so-called "case b" representations in Wigner's classification scheme. Here, this means that they are coupled together to a two-dimensional irrep if time-reversal is active, a behavior which is independent of the number of the spectroscopically active electrons of the material. Thus, we have a double degeneracy for those states that belong to $^2\Gamma_3$ and $^2\Gamma_4$. On the other hand, the

TABLE 2
Character Table of the Double Group $^2D_3$

$^2D_3$	$K_1^{(1)}$ (e)	$K_2^{(2)}$ (q)	$K_3^{(6)}$ (a, b)	$K_4^{(3)}$ (aq, bq)	$K_5^{(4)}$ (k, lq, mq)	$K_6^{(4)}$ (kq, l, m)	
$^2\Gamma_1$	1	1	1	1	1	1	
$^2\Gamma_2$	1	1	1	1	−1	−1	z R_z
$^2\Gamma_3$	1	−1	−1	1	$+i$	$-i$	} +3/2, −3/2, +9/2, −9/2,
$^2\Gamma_4$	1	−1	−1	1	$-i$	$+i$	} +15/2, −15/2
$^2\Gamma_5$	2	2	−1	−1	0	0	(x, y) (R_x, R_y)
$^2\Gamma_6$	2	−2	1	−1	0	0	±1/2, ±5/2, ±7/2, ±11/2, ±13/2, ±17/2

Note. The periods of the elements in the six classes K_1–K_6 are indicated as superscripts. The group elements of each of the classes are given in brackets below the corresponding class symbols. In the last column basis functions are given; half − odd integer values denote the M-values of the $|J, M\rangle$ basis functions.

TABLE 3
Selection Rules for Electric Dipole Transitions of Nd^{3+} Ions in $^2D_3$ Symmetry

		Final state	
		$(^2\Gamma_3, {}^2\Gamma_4)$	$^2\Gamma_6$
Initial	$(^2\Gamma_3, {}^2\Gamma_4)$	π	σ
State	$^2\Gamma_6$	σ	σ, π

Note. The irreducible representations are labelled according to Table 2.

defining representation $^2\Gamma_6$ belongs to the "case c" type which leads to no additional degeneracy for an odd number of active electrons. Finally, the remaining irreps of $^2D_3$ belong to the "case a" type which implies for an odd number of active electrons also a doubling of the original spatial degeneracy.

The relevance of a character table for spectroscopy lies, of course, mainly in the prediction of specific selection rules that can be obtained from the direct product of the representations for the initial and final state, and the relevant transition operator that couples these two states. The selection rules as well as the polarization of electric dipole transitions between two crystal field states of the Kramers-ion Nd^{3+} are summarized in Table 3.

3.2. Crystal Field States and Their Group Theoretical Assignment

Before selection rules can be applied the nature of the states involved in an observed transition (i.e., the irreps they span) has to be determined. This is a task far from trivial which is often based on some initial guesses, whose consistency is then checked against the outcome of the selection rules.

3.2.1. The $^4I_{9/2}$ Ground State Multiplet—Luminescence Spectroscopy. The laser-excited $^4F_{3/2} \rightarrow {}^4I_{9/2}$ luminescence spectrum of an Nd^{3+}:YAB (20 mol%) crystal recorded at room temperature is given in Fig. 2. It consists of a number of more or less resolved emission bands corresponding to transitions from the two crystal field components of the $^4F_{3/2}$ multiplet (denoted as a′ and b′ in Table 4) to the five crystal field components of the $^4I_{9/2}$ ground state multiplet. Seven band positions are easily detectable from Fig. 2. A more detailed analysis of the $^4F_{3/2} \rightarrow {}^4I_{9/2}$ luminescence spectrum reveals a weak feature in between the most intense band (indicated as "6" in Fig. 2) and the double band (bands "8" and "9"). Furthermore, band "6" is asymmetric and has a shoulder on its high-energy side. These two additional transition bands are indicated as "7" and "5" in Fig. 2, respectively.

The transition at the highest energy (band "1") has to be $^4F_{3/2}$(b′) $\rightarrow {}^4I_{9/2}$(a), denoted as (b′,a) in Table 4. If the next one is assumed to be $^4F_{3/2}$(a′) $\rightarrow {}^4I_{9/2}$(a), denoted as (a′,a), the splitting of the two crystal field components of the $^4F_{3/2}$ multiplet is found to be 52 cm^{-1}. This value is in excellent agreement with the experimentally determined splitting of 49 cm^{-1} of Ref. (1). Taking therefore the energies of the a′ and b′ components of $^4F_{3/2}$ as 11,390 and 11,442 cm^{-1}, respectively, we are now able to proceed with the assignment of the $^4F_{3/2} \rightarrow {}^4I_{9/2}$ spectrum and to obtain the energetic structure of the $^4I_{9/2}$ multiplet (given as version I in Table 4).

The result of this sort of deconvolution, however, is not unambiguous. The assignments given in Table 4 corroborate a crystal field splitting of the ground state in our crystals which corresponds closely to the one reported in Ref. (1). Note, however, that this assignment scheme involves only seven of the nine transition bands and that three transitions starting from different levels are coincident. An alternative assignment based on the same

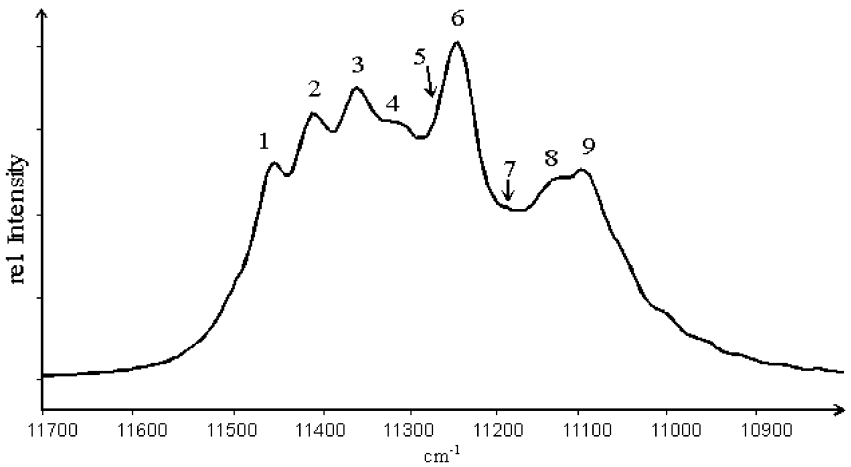

FIG. 2. $^4F_{3/2} \rightarrow {}^4I_{9/2}$ luminescence spectrum of Nd^{3+}:YAB (20 mol%) recorded at 300 K.

TABLE 4
Transition Bands According to the $^4F_{3/2} \rightarrow {}^4I_{9/2}$ Luminescence Spectrum of Fig. 2

		Version I				Version II			
Band	cm^{-1}	Assignment		$^4I_{9/2}$ splitting		Assignment		$^4I_{9/2}$ splitting	
1	11,442	(b′, a)	–	**0**	–	(b′, a)	–	**0**	–
2	11,390	(b′, b)	(a′, a)	**52**	**0**	(b′, b)	(a′, a)	**52**	**0**
3	11,338	(b′, c)	(a′, b)	**104**	**52**	–	(a′, b)	–	**52**
4	11,287	(b′, d)	(a′, c)	**155**	**103**	(b′, c)	–	**155**	–
5	11,236	–	(a′, d)	–	**154**	–	(a′, c)	–	**154**
6	11,223	–	–	–	–	(b′, d)	–	**219**	–
7	11,173	–	–	–	–	–	(a′, d)	–	**217**
8	11,136	(b′, e)	–	**306**	–	(b′, e)	–	**306**	–
9	11,099	–	(a′, e)	–	**291**	–	(a′, e)	–	**291**

Note. The different assignments (versions I and II) in terms of transitions starting from $^4F_{3/2}$(b′) and $^4F_{3/2}$(a′) are given together with the corresponding $^4I_{9/2}$ ground state splittings.

experimental data which has only one coincidence and includes all of the nine detected transitions is presented as version II in Table 4. In this case, however, a different ground state splitting is obtained.

While both sets of $^4I_{9/2}$ crystal field levels are consistent with the room-temperature luminescence spectra we strongly favor the set given as version II (Table 4) because it is also consistent with the results of the polarized absorption spectroscopy of the hot-band system $^4I_{9/2} \rightarrow {}^2P_{1/2}$ described below.

3.2.2. The $^4I_{9/2}$ Ground State Multiplet—Absorption Spectroscopy. Apart from a general increase of the absorbance due to the higher Nd^{3+} content in the Nd^{3+}:YAB (40 mol%) crystals the relative intensities in the absorption spectra of crystals doped with 20 and 40 mol% Nd^{3+} were identical. The $^4I_{9/2}$ ground state splitting can be obtained by polarized absorption spectroscopy using the hot-band system $^4I_{9/2} \rightarrow {}^2P_{1/2}$ at different temperatures between 10 K and room temperature (Fig. 3). Note that the $^2P_{1/2}$ multiplet consists of two components which remain Kramers-degenerate in crystal fields—this level is therefore always unsplit. In absorption spectra recorded at 10 K, where only the lowest crystal field state $^4I_{9/2}$(a) is populated, one single transition is observed. This single line appears in σ- as well as in π-polarized spectra. Since the nature of $^2P_{1/2}$ is $^2\Gamma_6$ (see Table 2) the nature of the state $^4I_{9/2}$(a) from inspection of Table 3 has to be $^2\Gamma_6$ as well. When the crystal is heated the higher Stark levels of the ground state multiplet $^4I_{9/2}$ become progressively populated and thus additional transitions—the so-called "hot bands" with initial states $^4I_{9/2}$(b), $^4I_{9/2}$(c), $^4I_{9/2}$(d), and $^4I_{9/2}$(e), respectively, to $^2P_{1/2}$—occur in the σ and π polarized absorption spectra (Fig. 3). In this way the energies and irreps of the ground state multiplet can be determined. The results are collected in Table 5.

The only problem occurs with the transitions starting from the $^4I_{9/2}$(d) and $^4I_{9/2}$(e) states. At the elevated temperatures necessary to observe these transitions their bands are too broad to be resolved. Furthermore, the intensity of the $^4I_{9/2} \rightarrow {}^2P_{1/2}$ transition is inherently very weak and the transitions from the higher components of the ground state multiplet are further decreased because of their low thermal population even at room temperature. In fact, the π-polarized spectra were too weak to be conclusive concerning these two levels. However, the σ-polarized absorption spectrum in combination with a peak fitting procedure can be used to work out the energies of $^4I_{9/2}$(d) and $^4I_{9/2}$(e) as 227 and 282 cm^{-1}, respectively.

Additional confirmation for the positions of the two components $^4I_{9/2}$(d) and $^4I_{9/2}$(e) are found from the hot

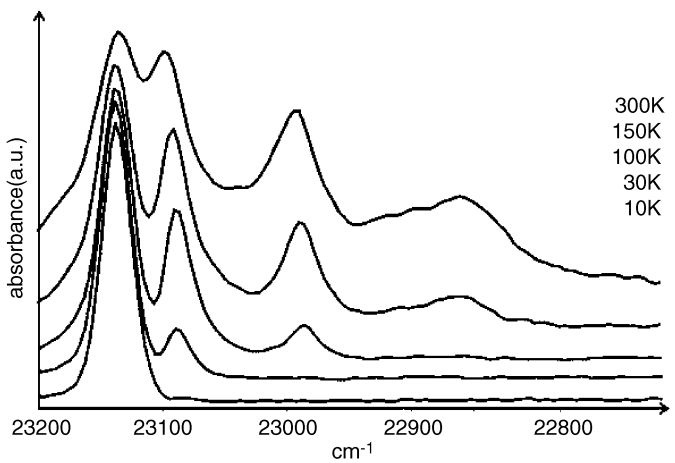

FIG. 3. Temperature dependence of the $^4I_{9/2} \rightarrow {}^2P_{1/2}$ transition in σ-polarization between 10 and 300 K. The most intense peak at 23,140 cm^{-1} is always displayed with the same intensity. For clarity, the hot-band spectra are slightly displaced along the absorbance axis.

TABLE 5

Transition Energies and Polarization of the Crystal Field Transitions $^4I_{9/2}$(a–e) → $^2P_{1/2}$ in the Absorption Spectra of Nd^{3+}:YAB(20 and 40 mol%), and Assignments of the $^2D_3$ Irreducible Representations

Transition (cm^{-1})	σ	π	States of $^4I_{9/2}$	Energy (cm^{-1})	$^2D_3$ assignments
23,140	+	+	a	0	$^2\Gamma_6$
23,090	+	–	b	49	($^2\Gamma_3$, $^2\Gamma_4$)
22,993	+	+	c	147	$^2\Gamma_6$
22,913	+	+	d	227	$^2\Gamma_6$
22,858	+	–	e	282	($^2\Gamma_3$, $^2\Gamma_4$)

bands to the transition of lowest energy in the $^4I_{9/2} \rightarrow {}^4G_{5/2}, {}^2G(2)_{7/2}$ region around 17,000 cm^{-1}. This region contains the most intense transitions of the Nd^{3+} absorption spectrum in the visible range. The hot bands originating from the $^4I_{9/2}$(d) and $^4I_{9/2}$(e) are indicated in Fig. 4 and are located at 16,647 and 16,592 cm^{-1}, respectively. This places them 225 and 280 cm^{-1} below the lowest energy transition at 16,873 cm^{-1} in the 10 K spectrum and hence nicely confirm the positions of both states as derived by the fitting of the $^2P_{1/2}$ hot bands.

Since in this spectral region also the π-polarized absorption spectra show enough intensity to analyze selection rules, the nature of the $^4I_{9/2}$(d) and $^4I_{9/2}$(e) states was assigned to $^2\Gamma_6$ and to the time-reversal coupled pair ($^2\Gamma_3$,$^2\Gamma_4$), respectively.

4. CONCLUSION

In Nd^{3+}:YAB the splitting of the $^4F_{3/2}$ state of about 50 cm^{-1} is similar to some energy differences between crystal field levels of the $^4I_{9/2}$ ground state manifold. For this reason, the $^4F_{3/2}$(a′,b′) → $^4I_{9/2}$(a, b, c, d, e) room-temperature luminescence spectrum is obscured by band coincidences. Thus, less than the 10 expected transitions are observed for this material. We have demonstrated in this work that this leaves room for ambiguous assignments of the ground state splitting. One method to overcome this problem is to record the $^4F_{3/2} \rightarrow {}^4I_{9/2}$ emission at low temperatures, where only transitions from the lower crystal field state of $^4F_{3/2}$ to the $^4I_{9/2}$ multiplet take place. However, the results for the $^4I_{9/2}$ ground field splitting obtained in this way are not always consistent throughout the literature (see references given in Table 1). In this contribution we have shown that in the case of Nd^{3+} temperature-dependent polarized absorption spectroscopy is a powerful method and an alternative to high-resolution low-temperature luminescence spectroscopy in order to assign the Stark levels of the $^4I_{9/2}$ ground state multiplet in terms of both their energies and their group theoretical nature (represented either by the irreducible representations which their wavefunctions span or by their crystal field quantum numbers) unambiguously. For our final result of the $^4I_{9/2}$ splitting pattern (Table 1) we have taken the energies of the lower crystal field levels $^4I_{9/2}$(a), $^4I_{9/2}$(b), and $^4I_{9/2}$(c) directly from the absorption experiment. For the dermination of the energies of the two remaining levels $^4I_{9/2}$(d) and $^4I_{9/2}$(e) we used a combination of the results obtained by fitting the high-temperature absorption spectra and of those obtained from the luminescence spectra of the $^4F_{3/2}$(a′) and $^4F_{3/2}$(b′) emissions (Table 4). For a consistent group theoretical assignment of the crystal field states (Table 5) it turns out that polarized absorption spectra recorded at different temperatures are sufficient.

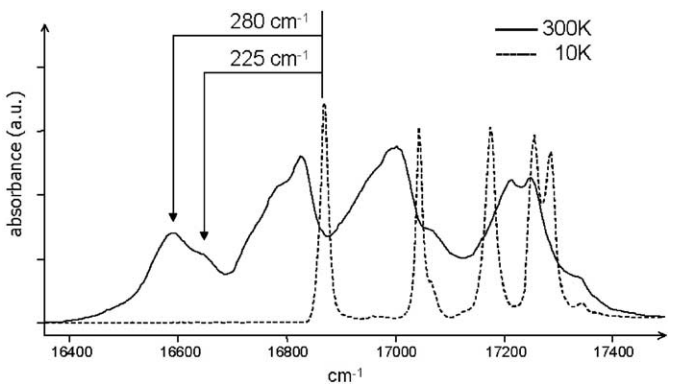

FIG. 4. The $^4I_{9/2} \rightarrow {}^4G_{5/2}, {}^2G(2)_{7/2}$ region in σ-polarization recorded at 10 and at 300 K.

REFERENCES

1. D. Jaque, J. Capmany, Z. D. Luo, and J. García Solé, *J. Phys.: Condens. Matter* **9,** 9715 (1997).
2. Chen Xueyuan and Luo Zundu, *J. Phys.: Condens. Matter* **10,** 5147 (1998).
3. D. Jaque, J. Capmany, F. Molero, Z. D. Luo, and J. García Solé, *Optical Materials* **10,** 211 (1998).
4. D. Jaque, J. Capmany, J. Rams, and J. García Solé, *J. Appl. Phys.* **87,** 1042 (2000).
5. Luo Zundu, Jiang Aidong, Huang Yichuan, and Qiu Minwang, *Chin. Phys. Lett.* **6,** 440 (1989).
6. D. Jaque, O. Enguita, U. Caldiño G., M. O. Ramírez, J. García Solé, C. Zaldo, J. E. Muñoz-Santiuste, A. D. Jiang, and Z. D. Luo, *J. Appl. Phys.* **90,** 561 (2001).
7. C. Cascales, C. Zaldo, U. Caldiño, J. García Solé, and Z. D. Luo, *J. Phys.: Condens. Matter* **13,** 8071 (2001).
8. Heng-fu Pan, Ming-guo Liu, Jing Xue, and Bao-sheng Lu, *J. Phys.: Condens. Matter* **2,** 4525 (1990).
9. S. Amano and T. Mochizuki, *Nonlinear Opt.* **1,** 297 (1991).
10. Yidong Huang and Zundu Luo, *Phys. Stat. Sol. B* **167,** K117 (1991).
11. Huang Yidong and Luo Zundu, *J. Phys.: Condens. Matter* **5,** 1581 (1993).
12. Luo Zundu and Huang Yidong, *J. Phys.: Condens. Matter* **5,** 6949 (1993).

13. G. Winzer, P. G. Mockel, and W. W. Kruhler, *IEEE J. Quantum Electron.* **14,** 840 (1978).
14. E. Antic-Fidancev, M. Lemaitre-Blaise, L. Beaury, G. Teste de Sagey, and P. Caro, *J. Chem. Phys.* **73,** 4613 (1980).
15. K. Gatterer, P. Day, H. P. Fritzer, and G. Sperka, *J. Mol. Struct.* **174,** 429 (1988).
16. K. Gatterer and H. P. Fritzer, *Phys. Chem. Miner.* **15,** 484 (1988).
17. A. A. Ballman, *Am. Mineral.* **47,** 1380 (1962).
18. S. T. Jung, D. Y. Choi, and S. J. Chung, *Mater Res. Bull.* **31,** 1007 (1996).
19. S. T. Jung, J. T. Yoon, and S. J. Chung, *Mater Res. Bull.* **31,** 1021 (1996).
20. E. Beregi, E. Hartmann, L. Malicskó, and J. Madarász, *Cryst. Res. Technol.* **34,** 641 (1999).
21. H. P. Fritzer, *Physica A* **114,** 477 (1982).
22. G. Herzberg, "Molecular Spectra and Molecular Structure; III. Electronic Spectra and Electronic Structure of Polyatomic Molecules." D. Van Nostrand Company, Princeton, 1966 (Table 50 in Appendix 1).
23. H. A. Bethe, *Ann. Phys.* **3,** 133 (1929).
24. W. Opechowski, *Physica* **7,** 552 (1940).
25. M. Tinkham, "Group Theory and Quantum Mechanics," p.141ff. McGraw-Hill, New York, 1964.